ISBN: 978-3-95450-231-8 ISSN: 2673-5490 doi: 10.18429/JACoW-IPAC2023-THPA011

STUDY OF NOISE IMPACT ON AI-BASED PTYCHOGRAPHY FOR BEAM CHARACTERIZATION

C. Sweeney†, S. Biedron[1] University of New Mexico, Albuquerque, USA
[1]also at Element Aero, Chicago, USA

Abstract

Ptychography is used to characterize coherent X-ray beam focus and to image nanoscale matter at light sources such as synchrotrons and free-electron lasers. Ptychography is a method for lensless imaging of a sample and can be performed via iterative algorithms and recently with AI-based methods. We study AI-based ptychographic image reconstruction from experimental X-ray diffraction patterns in the presence of additive noise and compare the effect of different noise types on the learning process and on inference. Experiments at the Advanced Photon Source (APS) provide the data and neural network for the study. Noise sources in the study include Poisson noise produced by quantization at the detector, Gaussian distributed shot-to-shot changes in total beam fluence (beam fluence jitter), and additive speckle.

INTRODUCTION

Lensless imaging is increasingly used to obtain resolution in the range of tens of nanometers or less, beyond the ability of the numerical aperture of a microscope lens. Synchrotron X-ray light sources and free-electron lasers can generate bright and coherent light beams that can be used to image samples. For thin samples, a method called ptychography ("ptych" is Greek for "to fold") can be used as described in [1, 2]. This method relies on imaging a sample at many overlapping regions, called scan points. See Fig. 1. The phase image of a sample is particularly useful for detecting differences in materials. Ptychography is also used for beam characterization. An amplitude image can be easily computed from the intensities of the diffraction pattern. However, the phase image is traditionally retrieved with computationally intensive and time-consuming iterative algorithms that leverage the region overlap.

Recently AI-based ptychographic methods have been explored [3-6] using encoder-decoder networks, convolutional generative adversarial networks, or a combination of AI and iterative methods. Samples include etched tungsten, human cancer cells, and simulated data from image datasets. These methods show great promise in quickly inferring phase images and reducing the number scan points needed for a reconstruction.

A number of noise sources occur in pytchographic setups in [7]. Some noise has been simulated by diffraction simulators for other applications [8] and to a limited extent by open-source ptychographic codes. Noise sources include noise from parasitic scattering (background), outliers, correlated noise sources, cosmic rays, bad frames, beam jitter, motor jitter, fluctuating dark noise, beam miscentering, static background and beam fluence jitter.

† csweeneynm@unm.edu

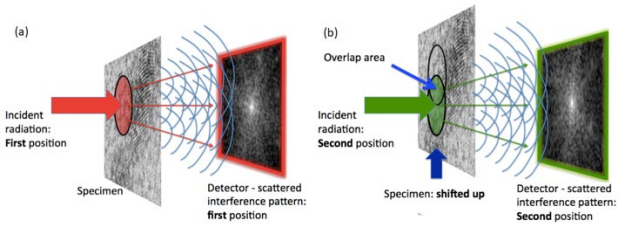

Figure 1: Cartoon of ptychography setup with (a) first position scanned and (b) second overlapping area scanned. Diffraction patterns are recorded on the detector behind the sample. Image from [9].

Little is known, however, about the impact of experimental noise on AI-based ptychography techniques. Knowing this impact could greatly improve research efforts in AI-based ptychography. We study the effect of random noise in experimental data used for AI-based ptychographic reconstruction. We assess how it impacts learning and inference (eg. the quality of the inferred reconstructed image). We use available ptychographic datasets from experiments performed by colleagues at the Advance Photon Source. We also use their neural network, PtychoNN [3].

METHODS

Noise can originate in the beam itself, elements along the beam path, the environment in the vicinity of the beam, sample, or detector, space (such as cosmic noise), the motors that move the sample in front of the beam, the camera readout, and the detector itself.

Table 1 lists the subset of different noise sources used in this study and what is required to simulate them. This information was gleaned from [7, 8, 10].

Neural Network and Data

We use the AI-based ptychography neural network called PtychoNN. The Python code and experimental data is available via open source at [11]. The network is an encoder-decoder convolutional network with 1,247,072 trainable parameters. The decoder part of the network has two arms, one to predict an amplitude image and one to predict a phase image. Both input training data images and output inferred images are 64x64 pixels.

We use the experimental dataset in [3] available at the same site as the code. The data are from experiments performed on etched Tungsten thin samples. The data include a 161x161 scan point square sample area. The top 100 lines of scan points (16,100) are used for training and the lower right 61x61 area is used for testing.

ISBN: 978-3-95450-231-8 ISSN: 2673-5490 doi: 10.18429/JACoW-IPAC2023-THPA011

Table 1: Noise in Diffraction

Type	Origin	Simulation
Photon count quantization noise (random)	Detector photon counting statistics	The noise takes a Poisson distribution
Additive Gaussian noise (random)	For noise testing purposes, artificial	Add Gaussian noise to randomly selected subset of diffraction pixels
Fluence jitter	Beam characteristics	Change beam fluence from shot-to-shot using a Gaussian distribution

Metrics

Mean-squared-error (MSE). For quality measurements, the study uses the MSE of the difference between the fully reconstructed predicted amplitude or phase images and the corresponding ground truth iteratively reconstructed images. Two MSE values, one for amplitude and one for phase are computed. An additional MSE metric is also computed with the idea that the fully reconstructed predicted images have enough overlap and pixel averaging that the previous MSE metric is not indicative of the direct impact of a noise on a particular predicted patch. It may make the reconstruction appear more resilient. Therefore, the MSE of the average difference between predicted amplitude and phase patches compared to ground truth is also computed.

Signal-to-Noise Ratio (SNR) metric. SNR is calculated as:

$$SNR = mean\left({O_g}^2\right)/MSE(O_g, O_p)$$

Where O_g is the ground truth object image and O_p is the predicted object image. SNR is computed for each fully reconstructed predicted amplitude image and phase image and then again for the average over the patches. The reason for computing SNR for the $O_g O_p$patches is similar to the reason for computing MSE on patches -- the individual patches do not have the redundancy, so a metric over those on their own could be useful.

Experiments

The experiments are described below with the name of the test in parentheses. This name is used in the plots in the results section.

Baseline Test. We use the original experimental data with thresholding of diffraction data that sets pixels below 3 to 0. This should remove some of the existing experimental Poisson noise.

Quantization Test. We use the original experimental data, but do not threshold pixels below 3, and add Poisson noise to all diffraction data (Poisson). An additional test (Poisson .01) is to scale down the photon counts by .01 and compute Poisson on that, then scale back. The rationale for this test is to create a larger jump in the counts when applied.

Fluence Tests. Use original experimental data, threshold as in the baseline, but multiply each pattern by fluence factor from Gaussian distribution with sigma at .1 and .5 for separate tests, factor is absolute value of the random number (Fluence.1 and Fluence.5).

Speckle Tests. Use original experimental data, threshold as in the baseline:

- Add photons of a random value distributed with Gaussian sigma at 130 or 260 (chosen because the average pixel value is 260 over all pixels in the experiment dataset) or 5000.
- Add the photons to a random number of pixels distributed with Gaussian sigma of 5% or 50% of the total pixels in a pattern (64x64) (Speckle 130-05, and Speckle 260-50).
- Space them according to uniform distributions between 0 and 63 for the y and x coordinates.
- As a second test, space them according to a Gaussian distribution between 0 and 63 with mean of 32 and clamped at x or y coordinates at 0 and 63 (SpeckleCenter 260 and SpeckleCenter 5000) (Fig. 2).

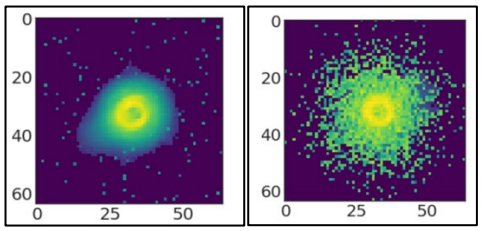

Figure 2: Diffraction with uniform (left) and spatially Gaussian distributed (right) speckle added.

Combination Test (Combo). Use original experimental data and do not threshold. Add speckle, then fluence and finally Poisson noise in that order, where fluence sigma is at .5, the speckle sigma for additive pixel value is at 130 and sigma for number of pixels to modify in a diffraction pattern is at .1x64x64.

RESULTS

The MSE results from the tests are summarized in Fig. 3 and Fig. 4. SNR results showed similar trends with low SNR when MSE was high and are not shown due to space.

The Baseline ground truth and diffraction dataset produce reconstructions of the test area with an average MSE (compared to ground truth) of 4.05E-5 for amplitude and .0915 for phase. Note that amplitude is much easier to reconstruct than phase with the AI-based method. That is also true for iterative reconstructions.

Quantization test results. For the Poisson random number generator on the data without scaling (the Poisson test), it showed little impact on the results. The metrics were very close to Baseline and the diffraction appeared unchanged.

For the Poisson random number generator on diffraction scaled down by .01 (the Poisson .01 test) then scaled back, it showed a bigger difference. The diffraction is noticeably different compared to the baseline dataset.

ISBN: 978-3-95450-231-8 ISSN: 2673-5490 doi: 10.18429/JACoW-IPAC2023-THPA011

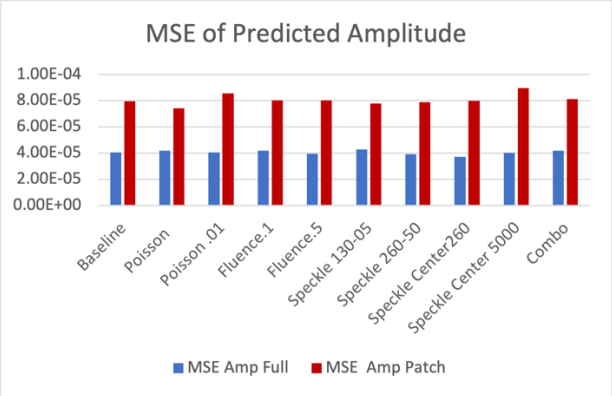

Figure 3: MSE of predicted amplitude shows steady values except for Poisson .01 and SpeckleCenter5000.

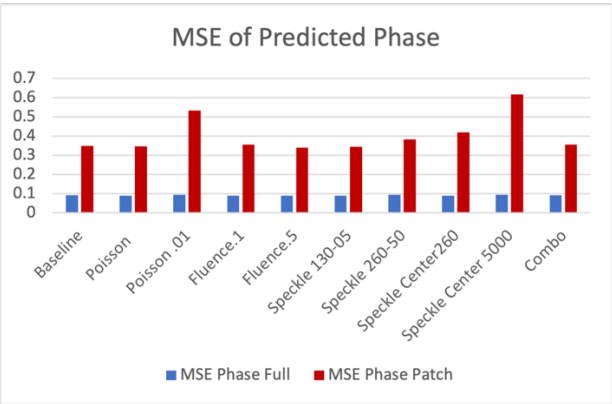

Figure 4: MSE of predicted phase shows variability in phase patch prediction.

The test area reconstruction for the Poisson .01 test has slightly degraded amplitude and phase MSEs as well as validation losses. The phase validation losses are over twice the baseline validation losses: they increased from .1398 to .3318. Some runs failed as early as Epoch 7, however, due to the training generating NaNs for the amplitude. Amplitude (intensities) can get quite high versus the phase numbers in the range of π to -π.

Fluence test results. This test thresholds experimental data as in the baseline, but it multiplies each pattern by fluence factor from a Gaussian distribution with sigma varying. For sigma at .1 and .5, these were small perturbations of the fluence and were not significantly different.

Speckle test results. The first Speckle tests uses the original experimental data, thresholds as in the baseline, adds photons of pixel value of sigma 130 or 260, and affects 50% of the pixels in a pattern uniformly spaced. This produces very little change even though visually it is apparent that speckle has been added as was shown in Fig. 2.

The second Speckle test adds higher intensity speckle noise with Gaussian sigma at 5000 to 50% of the pixels and with Gaussian spacing. It produces both visual confirmation of noise and a noticeable degradation in reconstruction as seen in Fig. 5, in several statistics including MSE for predicted phase patches, and in validation loss for phase.

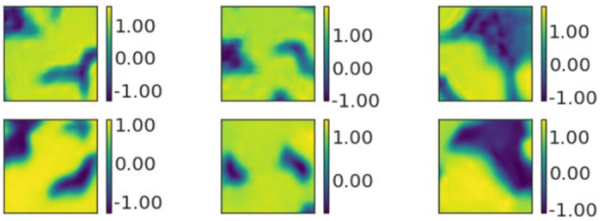

Figure 5: Patch results for true phase (above) and predicted phase (below) for SpeckleCenter 5000 noise test.

Combo test results. Overall, the amplitude and phase are very stable with the introduction of this combination of noise. This test could likely be made more impactful by increasing noise using a combination of Poisson at the .01 scaling, Fluence at .5 Gaussian sigma, and Speckle with the Gaussian sigma of 5000 for intensity and Gaussian spatial placement.

CONCLUSION

Results show that phase images, whether noisy or clean, are more difficult to train and predict versus amplitude images. This is seen in the higher MSE for phase full images and patches and lower SNR numbers for phase images. Some noise sources such as the Poisson .01 and Speckle Center tests affect predicted phase more than amplitude.

Our results also show that the redundancy provided by ptychography is very resilient to noise in stitched, averaged full predicted images, because it requires noise to be present in the same way in several overlapping patches. Less redundancy occurs if fewer samples are used, or there are many missing shots in a dataset.

Noise that affects more of the signal in the center seems to be impactful.

Much of the detected effect of noise in the predicted images was not noticeable by sight. SpeckleCenter 5000, however, shows some artifacts in predicted images.

Although some noise sources appeared to have more of an effect than others, the results are probably somewhat data-dependent and experiment-dependent. Future work will address this.

ACKNOWLEDGEMENTS

We acknowledge the help of Dr. Tao Zhou, who consulted on the use of PtychoNN and on preparing training data, Dr. Stefano Marchesini, who suggested ways to simulate noise, and Dr. Balusubramian Santhanam, who provided feedback on this project.

REFERENCES

[1] J. Rodenburg and A. Maiden, "Ptychography," in *Springer Handbook of Microscopy*, P. W. Hawkes and J. C. H. Spence, Eds., in Springer Handbooks. Cham: Springer International Publishing, 2019, pp. 819–904. doi:10.1007/978-3-030-00069-1_17.

[2] F. Pfeiffer, "X-ray ptychography," *Nat. Photonics*, vol. 12, no. 1, pp. 9–17, Jan. 2018, doi:10.1038/s41566-017-0072-5.

ISBN: 978-3-95450-231-8 ISSN: 2673-5490 doi: 10.18429/JACoW-IPAC2023-THPA011

[3] M. J. Cherukara *et al.*, "AI-enabled high-resolution scanning coherent diffraction imaging," *Appl. Phys. Lett.*, vol. 117, p. 044103, 2020. doi:10.1063/5.0013065.

[4] Z. Guan, E. H. R. Tsai, X. Huang, K. G. Yager, and H. Qin, "PtychoNet: Fast and High Quality Phase Retrieval for Ptychography," in Proc. *British Machine Vision Conference*, Cardiff, UK, Sep. 2019, p. 1172.

[5] T. Nguyen, Y. Xue, Y. Li, L. Tian, and G. Nehmetallah, "Deep learning approach for Fourier ptychography microscopy," *Opt. Express*, vol. 26, p. 26470, 2018. doi:10.1364/OE.26.026470.

[6] S. Welker, T. Peer, H. N. Chapman, and T. Gerkmann, "Deep Iterative Phase Retrieval for Ptychography," in Proc. *ICASSP 2022 - 2022 IEEE International Conference on Acoustics, Speech and Signal Processing (ICASSP)*, Singapore, May 2022, pp. 1591–1595. doi:10.1109/ICASSP43922.2022.9746811.

[7] H. Chang *et al.*, "Advanced Denoising for X-ray Ptychography," *Opt. Express*, vol. 27, p. 10395, 2019. doi:10.1364/OE.27.010395.

[8] A. Peck *et al.*, "Skopi: a simulation package for diffractive imaging of noncrystalline biomolecules," *J. Appl. Crystallogr.*, vol. 55, pp. 1002-1010, 2022. doi:10.1107/S1600576722005994.

[9] "Ptychography," *Wikipedia*. Jun. 30, 2022. Accessed: Jul. 26, 2022. https://en.wikipedia.org/w/index.php?title=Ptychography&oldid=1095727523

[10] V. Favre-Nicolin *et al.*, "PyNX: high-performance computing toolkit for coherent X-ray imaging based on operators," *J. Appl. Crystallogr.*, vol. 53, pp. 1404-1413, 2020. doi:10.1107/S1600576720010985.

[11] M. Cherukara et al., "PtychoNN," *GitHub*. https://github.com/mcherukara/PtychoNN (accessed Jul. 30, 2022).